


 Cite this: *RSC Adv.*, 2021, 11, 6423

Novel and versatile artificial intelligence algorithms for investigating possible GHSR1 α and DRD1 agonists for Alzheimer's disease†

 Zi-Qiang Tang,^{‡,a} Lu Zhao,^{‡,ab} Guan-Xing Chen^a and Calvin Yu-Chian Chen  ^{*acd}

Hippocampal lesions are recognized as the earliest pathological changes in Alzheimer's disease (AD). Recent researches have shown that the co-activation of growth hormone secretagogue receptor 1 α (GHSR1 α) and dopamine receptor D1 (DRD1) could recover the function of hippocampal synaptic and cognition. We combined traditional virtual screening technology with artificial intelligence models to screen multi-target agonists for target proteins from TCM database and a novel boost Generalized Regression Neural Network (GRNN) model was proposed in this article to improve the poor adjustability of GRNN. *R*-square was chosen to evaluate the accuracy of these artificial intelligent models. For the GHSR1 α agonist dataset, Adaptive Boosting (AdaBoost), Linear Ridge Regression (LRR), Support Vector Machine (SVM), and boost GRNN achieved good results; the *R*-square of the test set of these models reached 0.900, 0.813, 0.708, and 0.802, respectively. For the DRD1 agonist dataset, Gradient Boosting (GB), Random Forest (RF), SVM, and boost GRNN achieved good results; the *R*-square of the test set of these models reached 0.839, 0.781, 0.763, and 0.815, respectively. According to these values of *R*-square, it is obvious that boost GRNN and SVM have better adaptability for different data sets and boost GRNN is more accurate than SVM. To evaluate the reliability of screening results, molecular dynamics (MD) simulation experiments were performed to make sure that candidates were docked well in the protein binding site. By analyzing the results of these artificial intelligent models and MD experiments, we suggest that 2007_17103 and 2007_13380 are the possible dual-target drugs for Alzheimer's disease (AD).

 Received 29th November 2020
 Accepted 18th January 2021

DOI: 10.1039/d0ra10077c

rsc.li/rsc-advances

1 Introduction

Alzheimer's disease (AD) is a progressive degenerative disease of the nervous system characterized by generalized dementia. The clinical symptoms include memory impairment, aphasia, dyslexia, visual spatial skills impairment, executive dysfunction, and personality and behavior changes. Although, so far, the mechanisms of AD are not completely clear and the existing drugs are effective only in alleviating symptoms and not cure them, it is already clear that early diagnosis and early therapy of AD play a significantly positive role in improving the prognosis of patients as well as reducing the disease burden.

In addition, with the development of computer technology, computer-aided diagnosis and drug discovery has become one of the hottest research topics in the diagnosis and therapy of AD.^{1,2}

Hippocampal lesions have been considered as the early and defining pathology of AD;³ recent researches have demonstrated that growth hormone secretagogue receptor 1 α (GHSR1 α) and dopamine receptor D1 (DRD1), which are profusely co-expressed in the hippocampus, are involved in pathological processes.^{4,5} Activated GHSR1 α could shift DRD1 from a G α s to a G α q state by forming GHSR1 α /DRD1 heterodimers, then regulates DRD1-mediated initiating hippocampal synaptic reorganization *via* the non-canonical G α q-Ca²⁺ signaling pathway, which results in the activation of Ca²⁺ dependent protein kinase II (CaMKII); the phosphorylation of CaMKII could activate the synaptic plasticity. However, a direct interaction of GHSR1 α with β -amyloid (A β) in the hippocampus of patients with AD has been reported recently, which inhibited the activation of GHSR1 α and prevented GHSR1 α /DRD1 heterodimerization, leading to compromised GHSR1 α regulation of DRD1 in the hippocampus of patients with AD. Several recent studies also show that the co-activation of GHSR1 α /DRD1 protects GHSR1 α from A β toxicity as well as prevents AD-mediated synaptic abnormalities and behavioral

^aArtificial Intelligence Medical Center, School of Intelligent Systems Engineering, Sun Yat-sen University, Shenzhen, Guangzhou 510275, China. E-mail: chenychian@mail.sysu.edu.cn

^bDepartment of Clinical Laboratory, The Sixth Affiliated Hospital, Sun Yat-sen University, Guangzhou, 510655, China

^cDepartment of Medical Research, China Medical University Hospital, Taichung 40447, Taiwan

^dDepartment of Bioinformatics and Medical Engineering, Asia University, Taichung, 41354, Taiwan

† Electronic supplementary information (ESI) available. See DOI: 10.1039/d0ra10077c

‡ These authors contributed equally to this work.



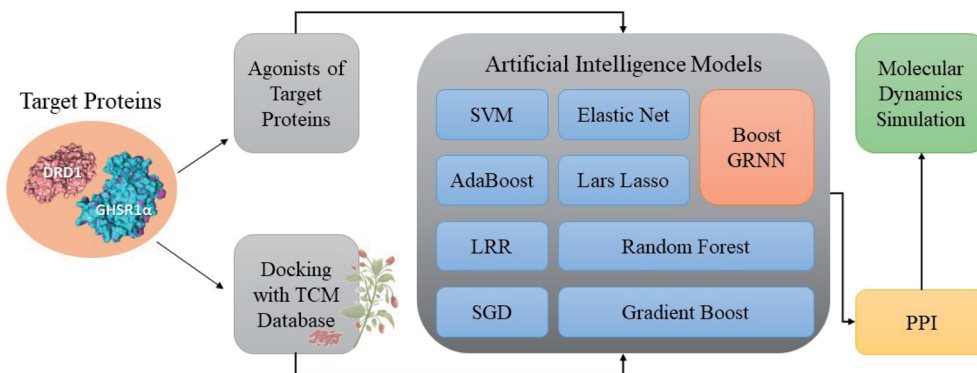


Fig. 1 Flow chart of the total experiment.

impairments in AD models.^{6,7} Even more interestingly, the new pathway has proved to be the cAMP-independent signaling pathway in the regulation of learning and memory, which is different from previous studies that have generally believed that AD is related to the cAMP signaling pathway.⁸ The proposal of the above studies provides a possible theoretical basis for the treatment of AD. We have been devoted to the computer-aided drug screening for many years.⁹ iScreen¹⁰ and iSMART¹¹ were applied for virtual drug screening and computer-aided drug design. Traditional Chinese Medicine (TCM) is an independent theoretical system totally different from western medicine and has made encouraging

achievements in the treatment of many diseases, especially chronic diseases, and has been applied widely. The TCM database¹² has been applied to the development and promotion of TCM as well as the discovery of potential new drug. In addition, artificial intelligence technology has been greatly developed due to a substantial increase in the computing power, which has laid the foundation for the “hardware” and “software” of computer-aided drug design, protein–protein interaction, and the prediction of target proteins.^{13–15} Therefore, we can easily predict drug activity,^{16,17} perform molecular dynamics (MD) simulation experiments^{18,19} for small molecules, and predict the drug targets.²⁰

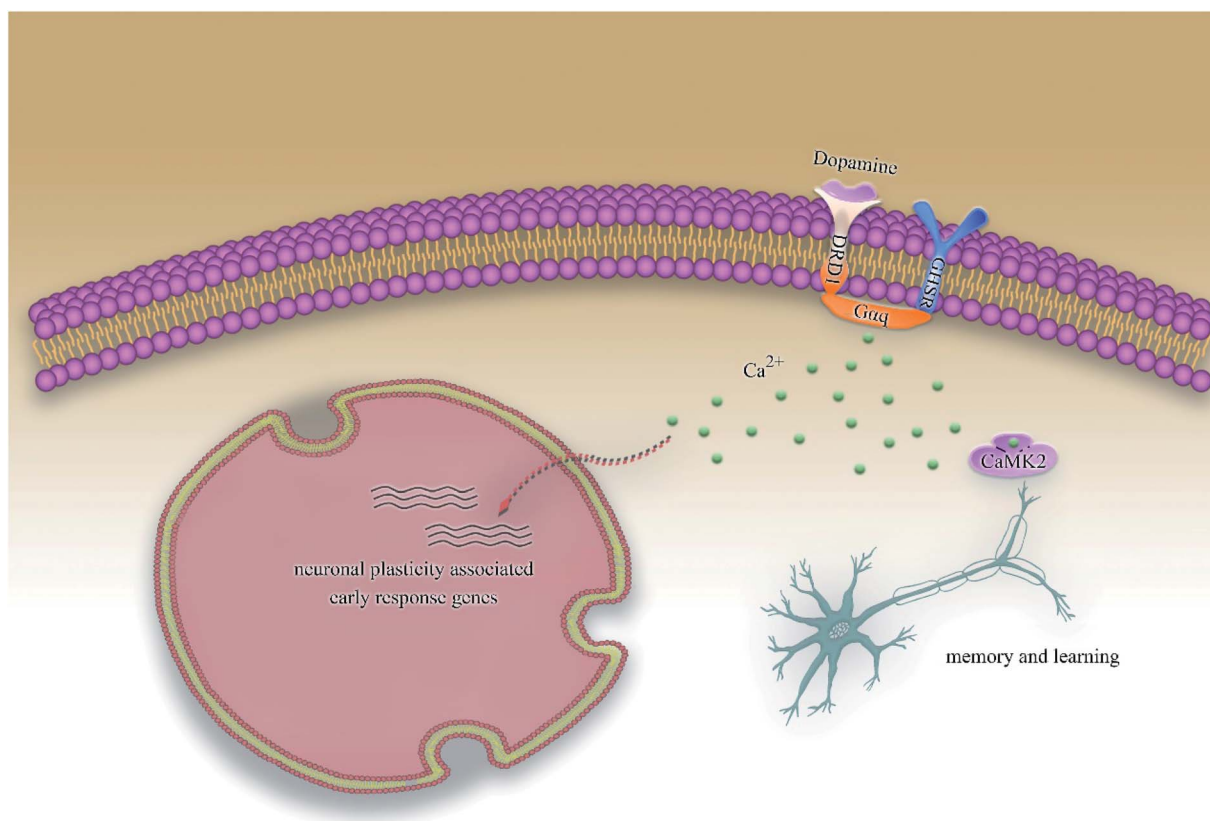


Fig. 2 The Alzheimer's disease pathway.



2 Materials and methods

Accumulating evidence suggests that the lack of GHSR1 α and DRD1 has a crucial role in the development of AD. Hence, in this paper, we chose nine artificial intelligent models to predict the drug activity for the new target proteins, which aims to identify the highest value of estimate binding affinity and the best docking score compounds from the TCM database that cloud activates the expressions of GHSR1 α and DRD1 for the treatment of AD. In order to solve the problem of the overfitting of small data sets and incomplete properties of multi-feature data sets, we propose a novel boost Generalized Regression Neural Network (GRNN). A further experiment, MD, was performed to verify whether these candidate compounds obtained from virtual screening can bind to the target protein stably. The flow chart of the entire experiment is shown in Fig. 1.

2.1 Network pharmacology analysis

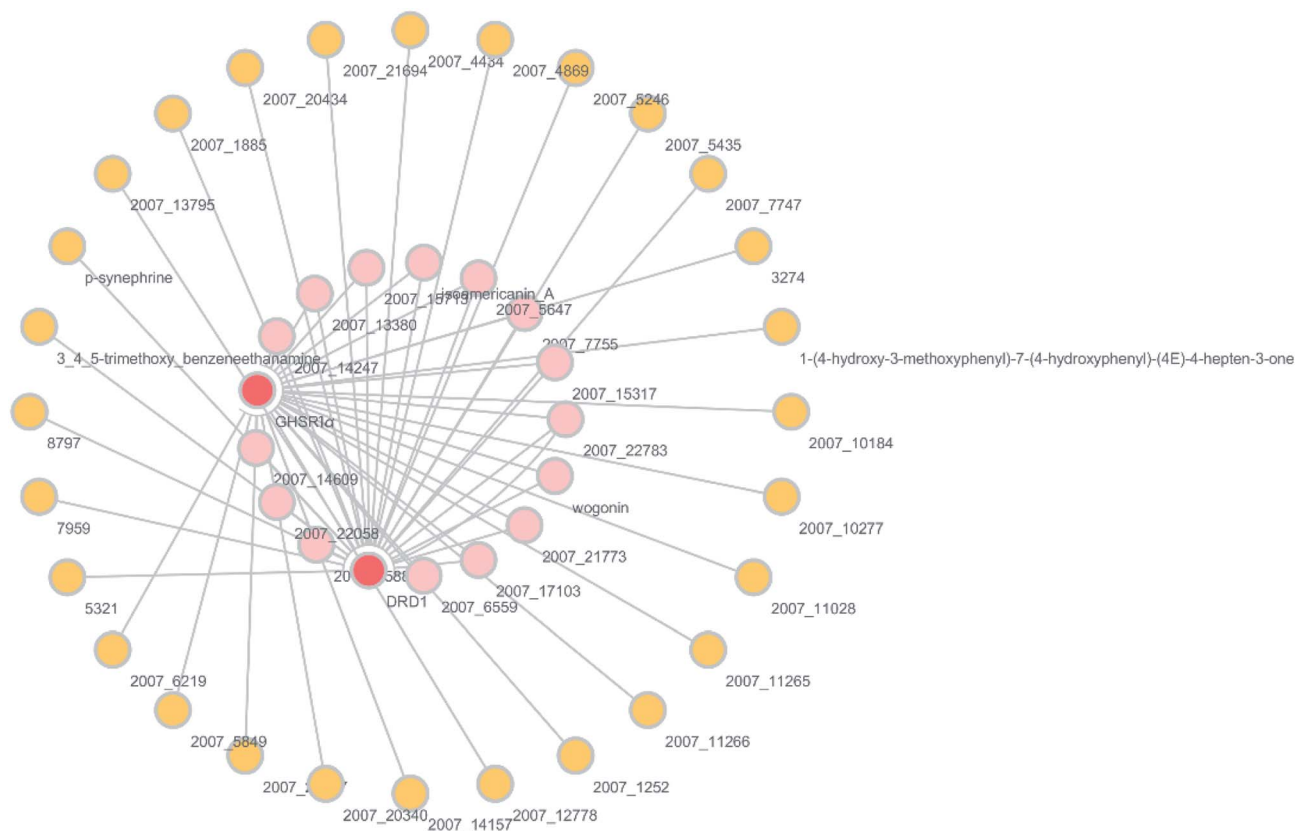
According to previous studies, we have determined that the target proteins are GHSR1 α and DRD1; signal transmission depends on G Protein-Coupled Receptors (GPCRs), especially GHSR1 α .^{4,6,7} Pathway data obtained from the novel research about AD and KEGG database²¹ was used to analyze the pathogenesis of AD, and the pathway diagram is shown in Fig. 2. GHSR1 α and DRD1 were docked with the TCM database. The

top 30 compounds from the TCM database with the dock scores were selected to draw the drug–protein interaction diagram by the Cytoscape software,²² which is shown in Fig. 3. Through the relevant research of the drug–protein interaction diagram, we are committed to finding out potential multi-target drugs that can interact with both GHSR1 α and DRD1 at the same time.

2.2 Screening and molecular docking

The crystal structures of DRD1 for AD were obtained from Protein Data Bank (PDB ID: 1oz5).²³ The protein sequences of GHSR1 α and DRD1 were derived from Uniprot Knowledgebase (Uniprot ID: Q92847, Q6FH34).^{24,25} We input the protein sequence and crystal structure of different target proteins into I-Tasser^{26–29} for homology modeling. Through I-Tasser's modeling process, the complete protein crystal structures and ligands of the target proteins were obtained. In specific experimental operations, we selected the modeling structures with the highest stability and reliability for the next experiment. In order to judge whether the proteins 3D model obtained from I-Tasser are reliable, we drew the Ramachandran plot diagram and 3D-profile diagram for the target proteins, which are shown in Fig. 4 and 5, respectively.

In order to make the target proteins more stable and reliable, the target proteins were removed from the crystal water and prepared by the Discovery Studio software (DS). At the same time, the ligands were used to define the binding sites of



different target proteins. The TCM database,¹² including 18 776 small molecules of Chinese herbal medicine ingredients, has proved to be the best choice for molecular docking experiments.^{30,31} The 'LigandFit module'³² was applied to dock the target proteins with the TCM database, which was included in the DS software. In our experiments, Chemistry at Harvard Macromolecular Mechanics (CHARMm27) was used to

preprocess the target proteins, which could minimize the docking pose.³³⁻³⁵ For different targets, according to the results of molecular docking, we selected the top 30 compounds with the highest molecular docking score as the input data of the artificial intelligent models. ADMET descriptors module in DS include absorption, distribution, metabolism, excretion, toxicity, and other information, which were used to describe

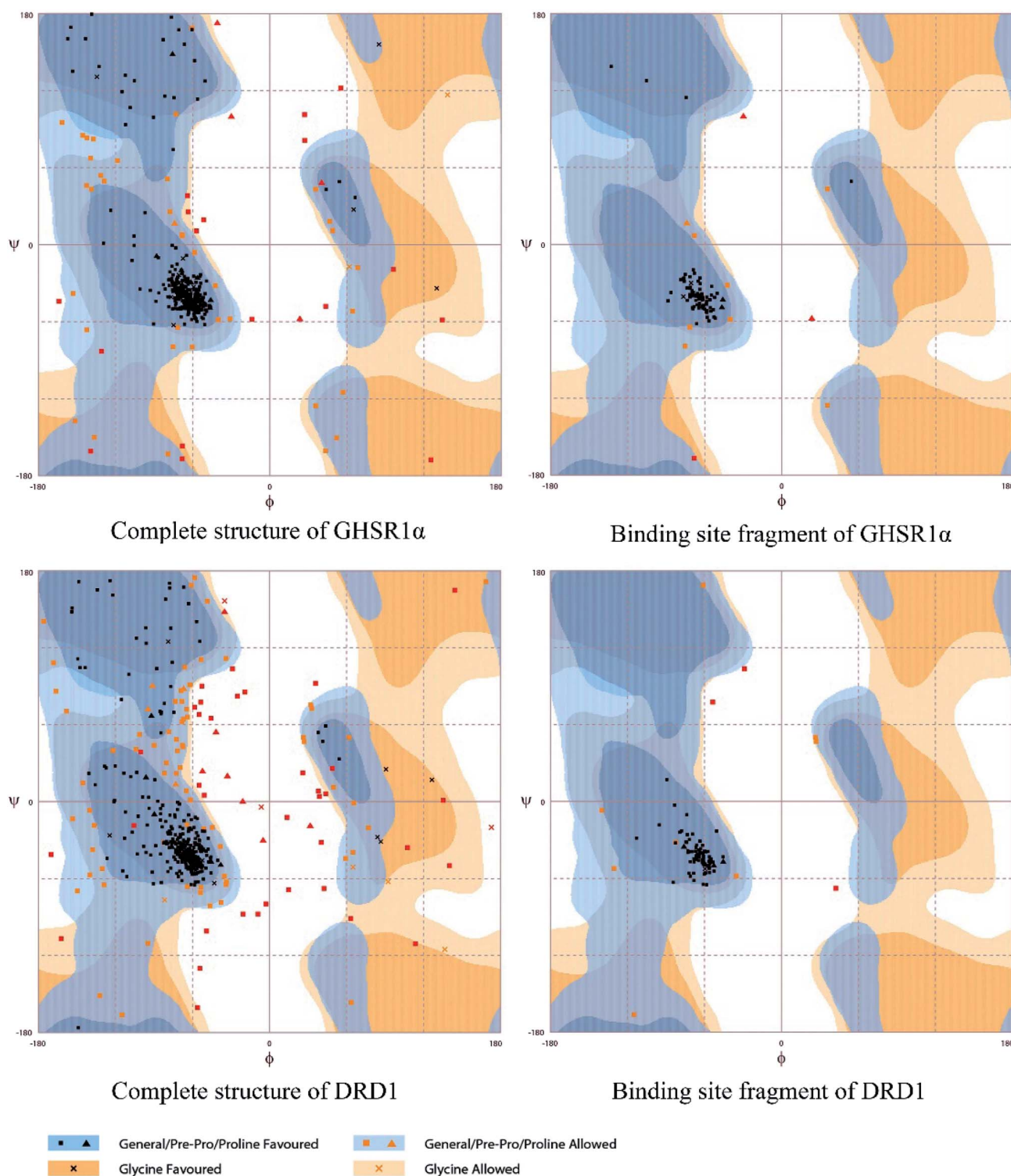


Fig. 4 Ramachandran plot results of the modeling structures.



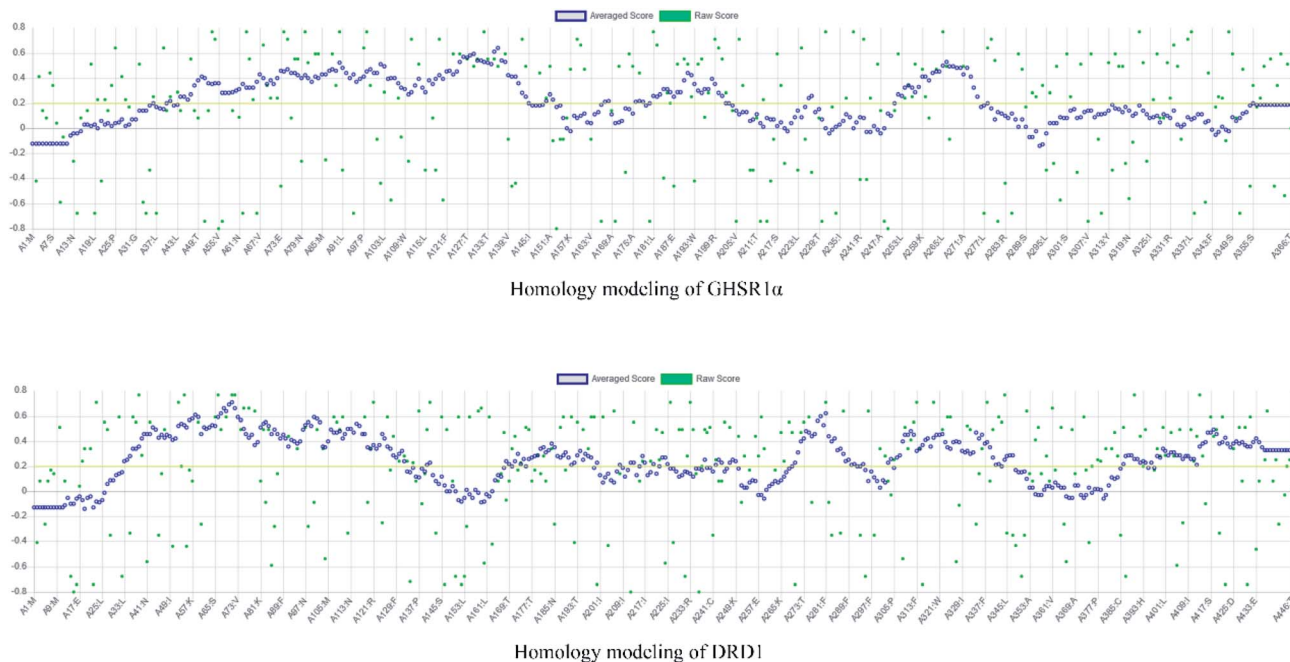


Fig. 5 3D-profile results of the homology modeling proteins.

and comprehensively analyze the solubility, blood–brain barrier (BBB) penetration, hepatotoxicity, and cytochrome P450 2D6 (CYP2D6) of small molecules in the TCM database.^{36,37} In addition, SwissADME³⁸ was used to judge whether the candidate compounds are the substrates of P-glycoprotein. According to the dock scores, ADMET descriptors results, and the predict results, we selected three possible candidates as the multi-target drugs for AD to perform the subsequent experiments.

2.3 Material and data preprocessing

The agonists of the target proteins came from the ChEMBL database.^{39,40} We used these compounds to calculate the

molecular properties. The number of these parameters describing molecular properties is as high as 204. During computer modeling, we selected the features so that the molecular features obtained can fit a more reasonable computer model. Excellent feature selection method is the basis to ensure the accuracy of the artificial intelligence models. We used Pearson correlation⁴¹ diagram to show the degree of correlation between each feature, which is shown in Fig. 6. Through this diagram, the relationship between each sample feature can be seen intuitively and it is clearly that there are quite a few molecular properties that are highly correlated with both the data sets of GHSR1 α and DRD1. In order to show the relationship between the high-dimensional pairwise features more

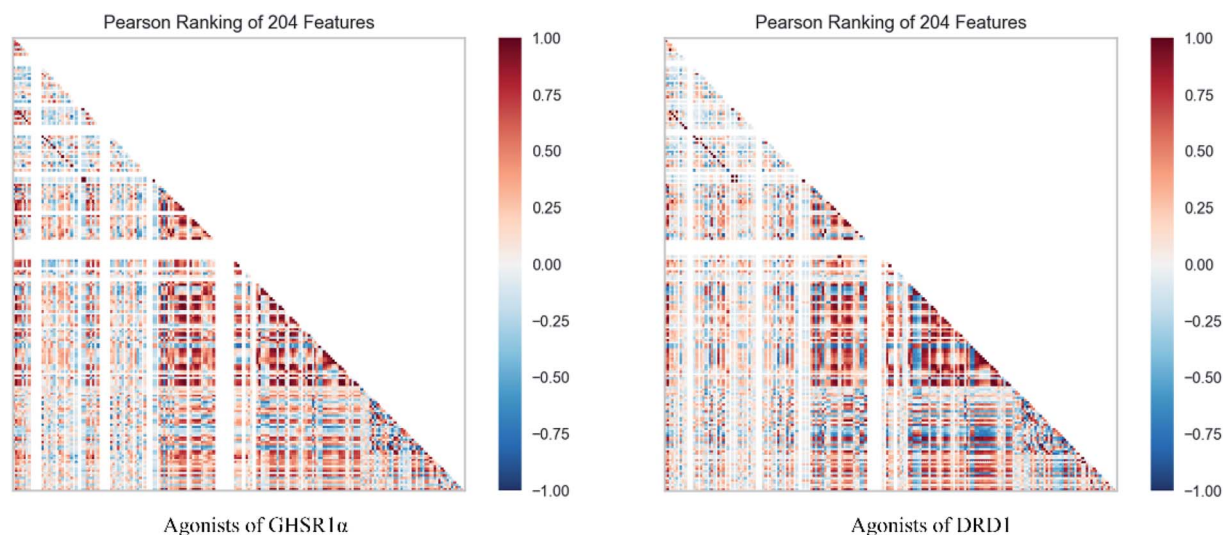


Fig. 6 Pearson correlation diagrams of 204 molecular properties.



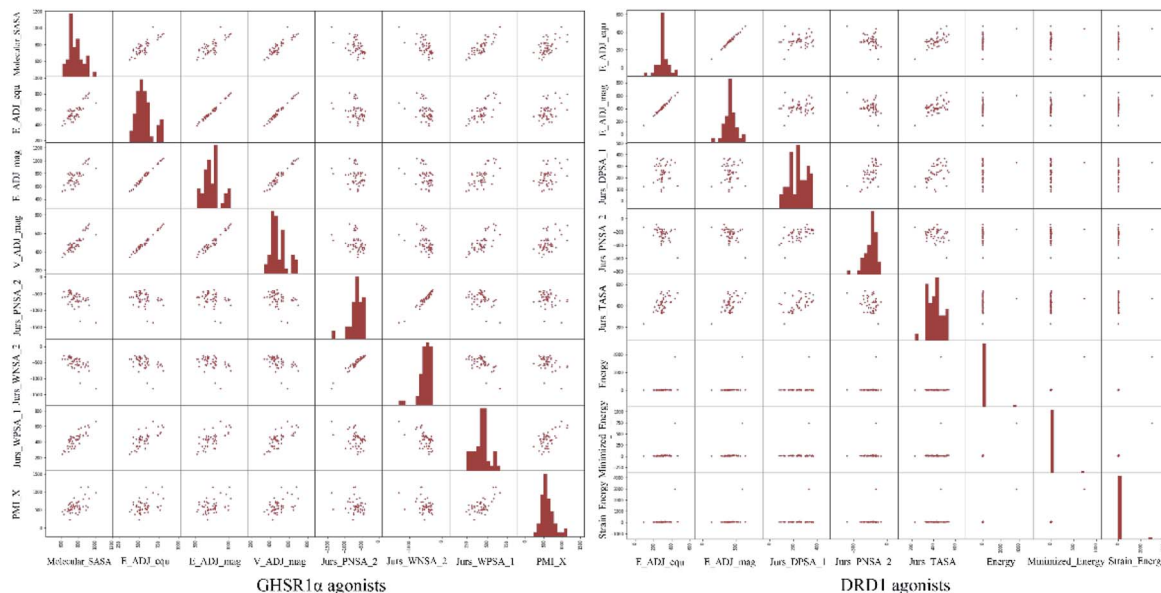


Fig. 7 Scatter matrix diagrams.

Algorithm: Adaptive Boosting

Initial weights $w_i = \frac{1}{N}, i = 1, 2, 3, \dots, N$

Repeat for $m = 1, 2, 3, \dots, M$

- Fit the classifier to obtain a class probability estimate.

$$p_m(x) = \hat{P}_w(y = 1|x) \in [0, 1]$$

$$f_m(x) \leftarrow \frac{1}{2} \log \frac{p_m(x)}{1 - p_m(x)} \in \mathbb{R}$$

- Set $w_i \leftarrow w_i \exp[-\gamma_i f_m(x_i)], i = 1, 2, 3, \dots, N$, and renormalize so that $\sum_i w_i = 1$.

Output:

$$\text{the classifier sign}[\sum_{m=1}^M f_m(x)].$$

Scheme 1 Training algorithm of adaptive boosting.

Algorithm: Gradient Boosting

Initialize:

$$f_0(x) = \arg \min_{\gamma} \sum_{x_i \in R_{j_m}} L(y_i, \gamma).$$

For $m = 1$ to M :

- For $i = 1, 2, 3, \dots, N$

$$r_{im} = -\left[\frac{\partial L(y_i, f(x_i))}{\partial f(x_i)} \right]_{f=f_{m-1}}$$

- Fit a regression tree to the targets r_{im} giving terminal regions $R_{jm}, j = 1, 2, 3, \dots, J_m$
- For $j = 1, 2, 3, \dots, J_m$

$$\gamma_{jm} = \arg \min_{\gamma} \sum_{x_i \in R_{j_m}} L(y_i, f_{m-1}(x_i) + \gamma)$$

$$f_m(x) = f_{m-1}(x) + \sum_{j=1}^{J_m} \gamma_{jm} I(x \in R_{j_m})$$

Output:

$$\hat{f}(x) = f_M(x)$$

Scheme 2 The algorithm of gradient boosting.



Algorithm: Elastic-Net

Input: $D = \{(x_1, y_1), (x_2, y_2), (x_3, y_3) \dots, (x_m, y_m)\}$

Loss function:

$$\min_w \frac{1}{2m} \sum_i (y_i - w^T x_i)^2$$

Objective function:

$$\min_w \frac{1}{2m} \left[\sum_i (y_i - w^T x_i)^2 + \lambda_1 \sum_{j=1}^n \|w\| + \lambda_2 \sum_{j=1}^n \|w\|_2^2 \right]$$

Output:

$$y = w^T x$$

Scheme 3 The algorithm of elastic-net.

Algorithm: Linear Ridge Regression

Input: $D = \{(x_1, y_1), (x_2, y_2), (x_3, y_3) \dots, (x_m, y_m)\}$;

Loss function:

$$\min_w \frac{1}{m} \sum_i (y_i - w^T x_i)^2 + \frac{\lambda}{n} \|w\|_2$$

Objective function:

$$\min_w \frac{1}{m} \sum_i (y - Xw)^T (y - Xw) + \frac{\lambda}{n} w^T w$$

Output:

$$y = w^T x$$

Scheme 4 The algorithm of linear ridge regression.

clearly, the scatter matrix diagrams were drawn based on the eight most relevant molecular properties. From the scatter matrix diagram, it can be clearly seen that there is a certain distribution correlation between each other of these molecular properties. The scatter matrix diagrams are shown in Fig. 7.

2.4 Molecular dynamics simulation

In order to evaluate whether the candidates could become possible drugs more accurately, we choose to conduct MD simulation experiments. By analyzing the results of MD simulations, we could effectively analyze the stability of the compounds and the target proteins' binding. We used

Algorithm: Support Vector Machine

Input: $D = \{(x_1, y_1), (x_2, y_2), (x_3, y_3) \dots, (x_m, y_m)\}$

Loss function:

$$\min_{w,b} \frac{1}{2} \|w\|^2 + C \sum_{i=1}^m l_\epsilon(f(x_i), y_i)$$
$$w = \sum_{i=1}^m (\hat{\alpha}_i - \alpha_i) x_i$$

Output:

$$f(x) = \sum_{i=1}^m (\hat{\alpha}_i - \alpha_i) x_i^T x + b$$

$$b = y_i + \epsilon - \sum_{i=1}^m (\hat{\alpha}_i - \alpha_i) x_i^T x$$

Scheme 5 The algorithm of support vector machine.

SwissParam web server to preprocess the candidates and generated the topology file, which provided a variety of information about the candidates including but not limited to atom type and bonding situation. Six 100 ns MD simulation experiments were implemented on the three candidates and two target proteins. The system temperature in NVT was set at 310 K for Maxwell distribution. Lincs constraint algorithm was adopted in these experiments to simulate the biological environment. Root mean square deviation (RMSD), total energy, the radius of gyrate, solvent-accessible solvent area (SASA), and root

mean square deviation (RMSF) were used for the verification of the results of the MD simulation experiments.

2.5 Artificial intelligence algorithms

2.5.1 Adaptive boosting. Adaptive Boosting (AdaBoost model)⁴² is used to superimpose different weak classifiers so that the training results and accuracy can meet the requirements. The samples with errors from the previous classifier are input into the next weak classifier as a new data set. The weights

Algorithm: Stochastic Gradient Descent

Input: Training set $R = \{x_1, x_2, x_3, \dots, x_i\}$

Logic regression:

$$f_{\epsilon}(x) = g(\epsilon^T x) = 1/(1 + e^{-\epsilon^T x})$$

Conditional probability:

$$h(p|x; \epsilon) = [f_{\epsilon}(x)]^p * [1 - f_{\epsilon}(x)]^{1-p}$$

Loss function:

$$L(\epsilon) = \prod_{i=1}^n h(p_i|x_i; \epsilon) = \prod_{i=1}^n [f_{\epsilon}(x_i)]^{p_i} * [1 - f_{\epsilon}(x_i)]^{(1-p_i)}$$

Logarithm transformation:

$$l(\epsilon) = \log L(\epsilon) = \sum_{i=1}^n p_i * \log f_{\epsilon}(x_i) + (1 - p_i) \log[1 - f_{\epsilon}(x_i)]$$

Maximum likelihood estimation:

$$l(\epsilon)_{max} \rightarrow J(\epsilon)_{min}$$

$$J(\epsilon) = -\frac{1}{n} l(\epsilon)$$

Iteration process:

$$\frac{\partial}{\partial \epsilon_j} J(\epsilon) = \frac{1}{n} \sum_{i=1}^n (f_{\epsilon}(x_i) - p_i) x_i^j$$

$$\epsilon_j = \epsilon_j - \alpha \frac{\partial}{\partial \epsilon_j} J(\epsilon) = \epsilon_j + \alpha \frac{1}{n} \sum_{i=1}^n (p_i - f_{\epsilon}(x_i)) x_i^j$$

Scheme 6 The algorithm of stochastic gradient descent.

Algorithm: Lasso

Input: $D = \{(x_1, y_1), (x_2, y_2), (x_3, y_3) \dots, (x_m, y_m)\}$;

Loss function:

$$\min_w \frac{1}{2m} \sum_i (y_i - w^T x_i)^2$$

Objective function:

$$\min_w \frac{1}{2m} \left[\sum_i (y_i - w^T x_i)^2 + \lambda_1 \sum_{j=1}^n \|w_j\| \right]$$

Output:

$$y = w^T x$$

Scheme 7 The algorithm of Lasso.



Algorithm: Random Forest

Input: $D = \{(x_1, y_1), (x_2, y_2), (x_3, y_3) \dots, (x_m, y_m)\}$;Basic algorithm \mathcal{L} : decision trees

- Repeat for $t = 1, 2, 3, \dots, T$
- $h_t = \mathcal{L}(D, D_{bs})$
- end for

Output:

$$H(x) = \arg \max_{y \in \mathcal{Y}} \sum_{t=1}^T \mathbb{I}(h_t(x) = y)$$

Scheme 8 The algorithm of random forest.

2.5.4 Linear ridge regression. Linear Ridge Regression (LLR) model⁴⁵ is a biased estimation regression method dedicated to collinearity data analysis. It is essentially an improved least squares estimation method, which obtains a good regression model through the loss of information. For biased data, this model can reduce the data noise very well and is more practical than other models.⁴⁶ In the process of the model training, we need to filter out the excellent features and discard the data noise. Therefore, this characteristic of the LLR model meets our experimental needs. The algorithm of LRR is given in Scheme 4.

2.5.5 Support vector machine. Support Vector Machine (SVM)⁴⁷ is a supervised learning model, which is usually used for classification. However, because of the prominent regression ability, this model can also be applied to the regression of complex features data sets, which is called Support Vector Regression (SVR).⁴⁸ Our input data includes 204 molecular characteristics, and the SVM model can obtain good prediction results and high reliability. The SVM model has a variety of kernel functions. In this experiment, the Gaussian (RBF)^{49,50} kernel function was adopted in consideration of the characteristics of our data sets. Facts have proved that the SVM model

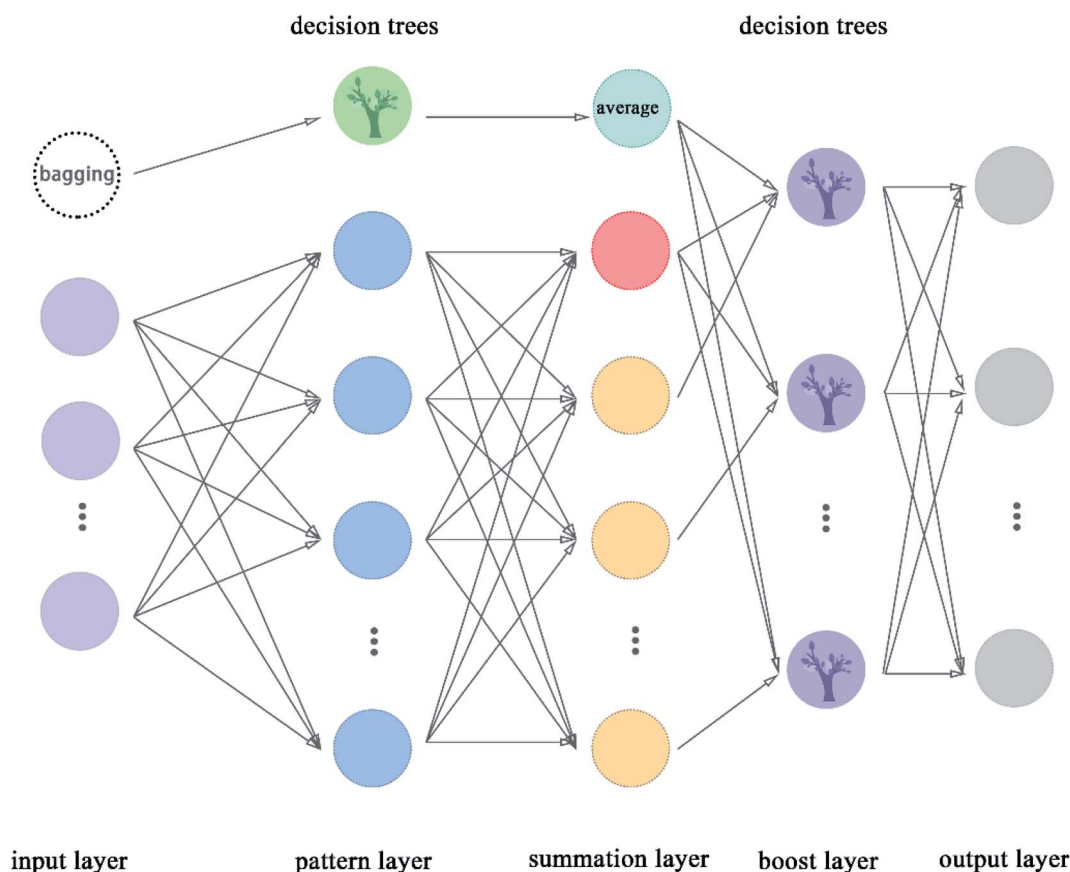


Fig. 10 Flowchart of boost GRNN.



2.5.8 Random Forest. Random Forest (RF) model⁵³ refers to a classifier that uses multiple decision trees to train and predict samples, which has also been applied in this paper. Each decision tree randomly selects the features included in the data set to classify and the classification of the next level decision tree is based on the features that the previous level decision tree has not used. Since each decision tree randomly introduces a subset of features as the classification index, the RF model easily avoids overfitting and has good anti-noise ability. Similarly, RF has good adaptability to multi-features. The flow chart of RF and the schematic diagram of bagging are shown in Fig. 8 and 9, respectively. The algorithm of RF is given in Scheme 8.

2.5.9 Boost generalized regression neural network. Boost GRNN model was proposed in this article by us to improve the adjustability of GRNN. Boost layer and first module were added in this model compared to the original GRNN.⁵⁴ The boost GRNN model includes input layer, pattern layer, summation layer, boost layer, and output layer. The input layer, pattern layer, and summation layer contain two modules. The first module takes multiple subsets of the input data set and uses decision trees for classification. The second module divides the input data set according to features and the number of nodes is equal to the number of features of the data set. The pattern layer of the first module classifies these samples according to the features. The pattern layer of the second module calculates the value of the Gauss function for each sample. The number of nodes of pattern layer is equal to the number of features except for the node with green color, which is called the decision trees. The decision trees are used to classify these subsets from the bagging node. The number of nodes in the summation layer is two more than the number of features. The extra node shown in indigo color represent the average value taken after the decision trees are classified. The extra node shown in red color in the flow chart is the arithmetic sum of the output of the pattern layer. The remaining nodes represent the weighted sum of nodes in the pattern layer. The boost layer uses the decision

trees to classify the data from the summation layer and get the required prediction values. We can adjust the number of decision trees in the boost layer to make the model get the best results. The flow chart of boost GRNN is shown in Fig. 10. The algorithm of boost GRNN is given in Scheme 9.

3 Results and discussion

3.1 Network pharmacology analysis

A large number of previous studies have shown that the combined activation of GHSR1 α and DRD1 is an effective treatment for AD.^{4,5,7,8} GHSR1 α and DRD1 were considered as the target proteins for molecular docking with the TCM database. We selected the top 30 small molecule compounds ranked by the docking score in the docking results for network pharmacology analysis. The drug-protein interaction diagram is shown in Fig. 3. According to the results of network pharmacology analysis, we can easily understand that 15 small molecule compounds can simultaneously interact with GHSR1 α and DRD1. These 15 compounds will be further analyzed to select the suitable candidates, which may be the possible drugs for AD.

3.2 Virtual screening

Through the drug-protein interaction diagram, we know that 15 compounds from TCM database can interact with two target

Table 2 Docking results of GHSR1 α and DRD1

Name	Dock score of GHSR1 α	Dock score of DRD1
2007_14247	121.472	114.392
2007_17103	108.997	114.699
2007_13380	114.163	110.554
2007_7588	133.836	113.422
2007_15317	129.466	108.701

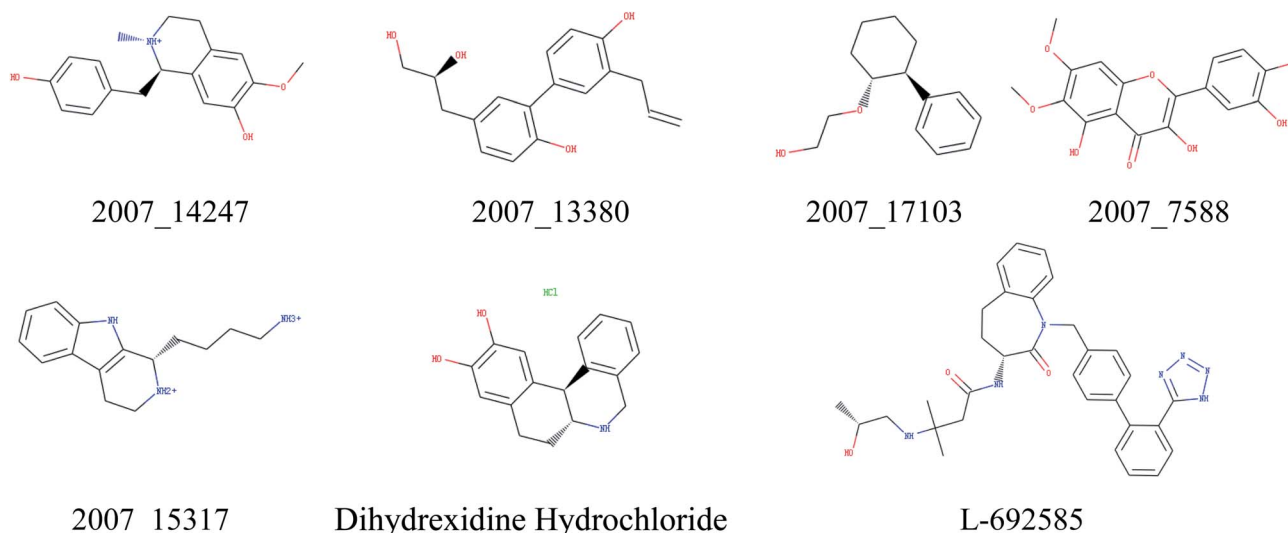


Fig. 11 Two-dimensional structures of the selected compounds and reference compounds.



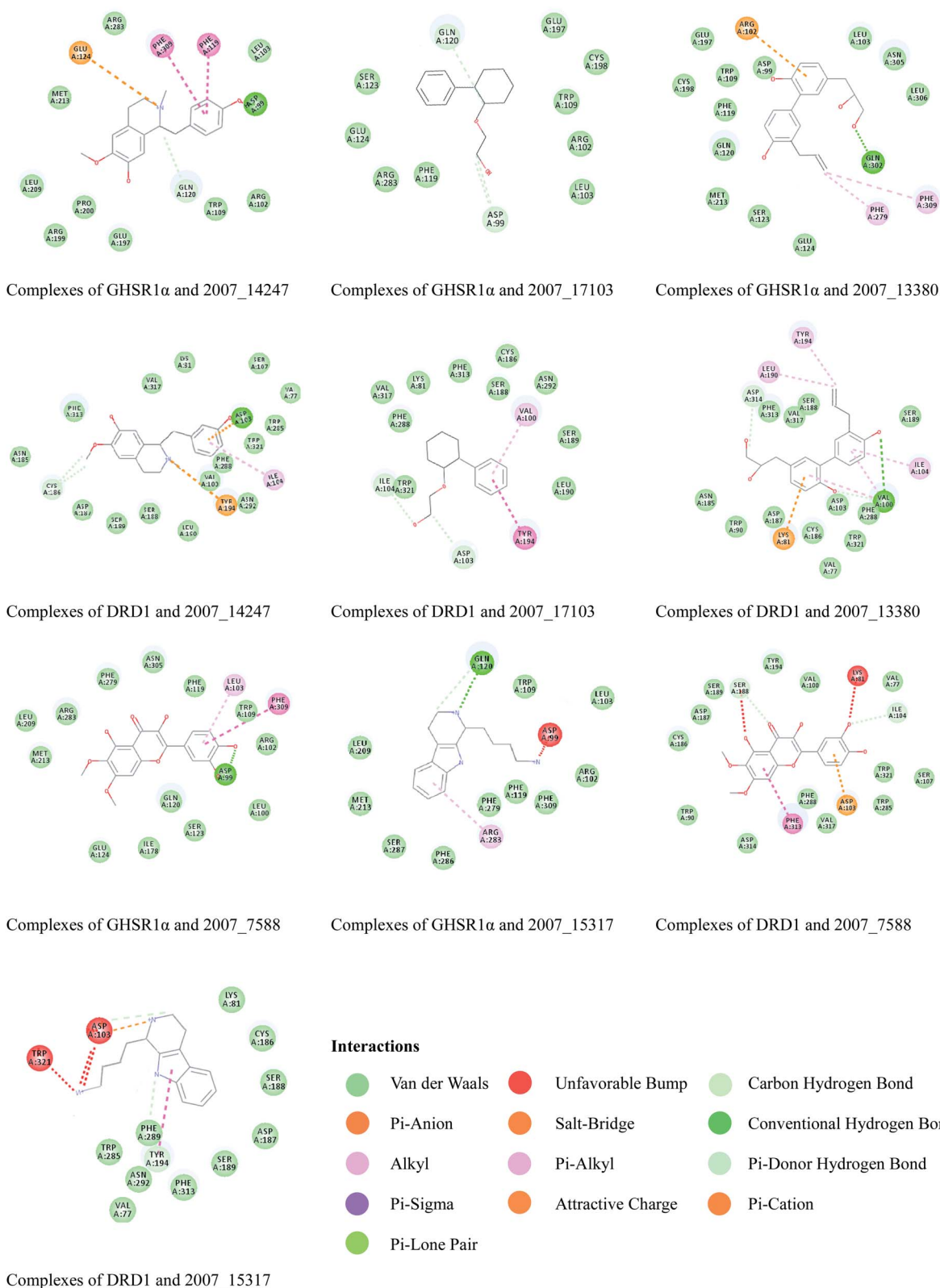


Fig. 13 2D diagrams of the compounds and target protein complexes.

relatively close. The details of reference compounds are given in Table 1. The two-dimensional structures of the selected compounds and the reference compounds are given in Fig. 11. The docking results of the candidates are shown in Table 2 and

Fig. 12. In order to evaluate the crystal structures of the target proteins, the 3D-profile diagrams were drawn. The results show that only a very small number of evaluation scores are less than 0, which means that our models are reasonable and reliable.



Table 3 Evaluation results of ADMET descriptors and substrate of P-glycoprotein

Name	Absorption	AlogP98	BBB level	CYP2D6	Hepatotoxicity	Log solubility	Substrate of P-glycoprotein
2007_14247	0	1.85	2	0	1	-2.342	Yes
2007_17103	0	2.72	1	0	0	-2.838	No
2007_13380	0	3.078	2	0	1	-2.244	No
2007_7588	1	1.84	4	0	1	-3.185	No
2007_15317	0	-0.017	3	1	0	-0.333	Yes

Table 4 Predicted activity values (predict pEC₅₀, nM), model training based on GHSR1 α agonists

Name	Model								
	AdaBoost	GB	EN	LRR	SVM	SGD	LL	RF	Boost GRNN
2007_14247	7.875	6.891	7.493	9.201	8.193	8.085	7.981	8.177	8.639
2007_17103	8.026	7.687	8.667	10.057	8.004	8.902	8.552	8.414	6.590
2007_13380	8.441	6.891	9.732	11.079	8.398	10.039	10.407	8.454	6.571
2007_7588	8.022	7.855	7.991	7.929	7.996	9.061	7.633	7.808	6.462
2007_15317	7.730	8.519	6.834	7.004	7.604	6.255	7.007	7.902	8.068

Table 5 Predicted activity values (predict pEC₅₀, nM), model training based on DRD1 agonists

Name	Model								
	AdaBoost	GB	EN	LRR	SVM	SGD	LL	RF	Boost GRNN
2007_14247	8.695	8.353	9.002	8.434	8.342	8.778	8.747	8.543	7.878
2007_17103	7.704	7.172	8.021	8.416	8.044	7.632	7.618	7.997	7.097
2007_13380	7.490	7.713	7.629	7.489	7.625	7.602	7.671	7.501	7.007
2007_7588	7.818	7.936	8.382	7.541	7.773	8.206	8.380	7.997	7.097
2007_15317	9.194	7.978	8.312	8.650	7.916	8.214	8.478	8.929	7.007

Ramachandran plot was used to analyze whether the amino acid conformation is reasonable. The results show that almost all the conformation points fall within the allowable range. Ramachandran plots and 3D-profile diagrams are shown in Fig. 4 and 5, respectively. Finally, we choose 2007_14247, 2007_17103, and 2007_13380 as the candidate compounds. The complexes formed by these compounds from the TCM database and the target proteins are displayed in Fig. 13. 2007_14247 formed a carbon-hydrogen bond with GLN120 of GHSR1 α at a distance of 2.27 Å and formed two carbon-hydrogen bonds with CYS186 of DRD1 at the same distance of 2.36 Å. 2007_17103 and GLN120 of GHSR1 α formed a carbon-hydrogen bond with a distance of 2.42 Å and two carbon-hydrogen bonds with APS99; the distances are 2.94 Å and 2.77 Å, respectively. 2007_17103 and ILE104, APS103 of DRD1 formed two carbon-hydrogen bonds with a distance of 2.15 Å and 2.91 Å, respectively. 2007_13380 formed a hydrogen bond with GLN302 of GHSR1 α at a distance of 1.5 Å and formed a hydrogen bond with VAL100 of DRD1 at a distance of 2.52 Å. 2007_15317 formed a 3.64 Å hydrogen bond with GHSR1 α but at the same time, it also formed a bond with a strong adverse effect; the unfavorable bond length is 3.19 Å. Unfortunately, this

compound forms three unfavorable bonds with DRD1. 2007_7588 and DRD1 formed two unfavorable bonds with GHSR1 α . Therefore, we will not consider these two compounds from the TCM database in the later experiments. In order to more accurately determine whether the compounds are the effective Chinese medicine herbs for the treatment of AD, we used the ADMET descriptors^{37,57} to further evaluate these

Table 6 Model evaluation results

Model	GHSR1 α		DRD1	
	R ² of training set	R ² of test set	R ² of training set	R ² of test set
AdaBoost	0.906	0.900	0.722	0.657
GB	0.935	0.785	0.976	0.839
EN	0.808	0.741	0.725	0.722
LRR	0.902	0.813	0.738	0.738
SVM	0.942	0.708	0.781	0.763
SGD	0.742	0.733	0.611	0.601
LL	0.827	0.801	0.688	0.511
RF	0.864	0.813	0.801	0.781
Boost GRNN	0.999	0.802	0.999	0.815



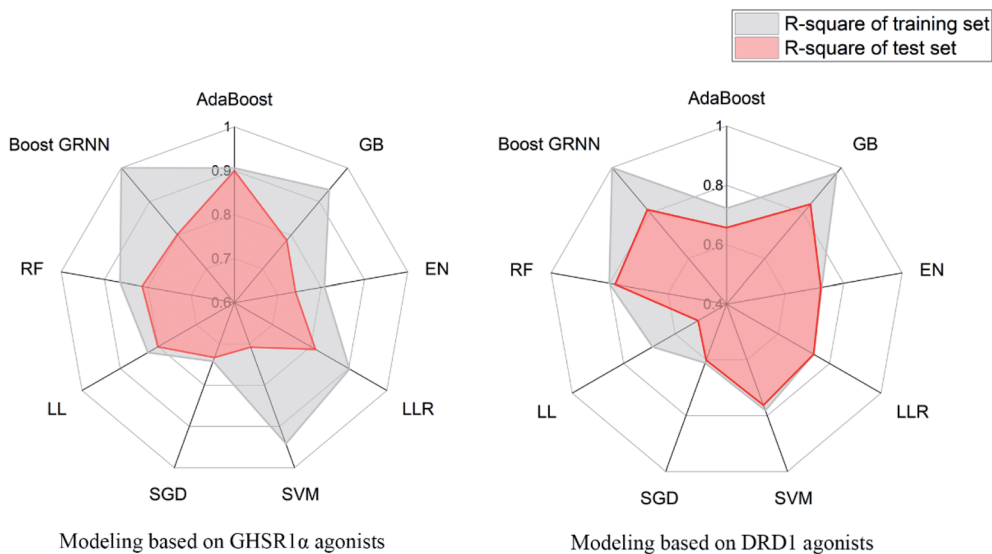


Fig. 14 Radar diagrams of the accuracy of each model.

compounds. The results of ADMET descriptors are shown in Table 3. The parameter of absorption was used to evaluate the pure passive transport of compounds across the membrane. According to the results of the absorption level, 2007_14247, 2007_17103, 2007_13380, and 2007_15317 have excellent absorption. AlogP98 was used to evaluate the lipophilicity, which is an evaluation index for the hydrophilicity of these compounds. Drugs that require a central nervous system can bind to the target proteins only after passing the BBB. Comparing the BBB level evaluation values of these compounds, we believed that the penetration ability of 2007_7588 and 2007_15317 is poor. The indicator of CYP2D6 reflects whether these compounds have an inhibitory effect on the CYP2D6 enzyme. Among these compounds, only 2007_15317 has an inhibitory effect on the CYP2D6 enzyme. Hepatotoxicity was used to verify whether the compound has

liver toxicity. The ADMET descriptor evaluation results shown that, except for 2007_17103 and 2007_15317, the other three compounds all have some hepatotoxic. The solubility parameter of the ADMET descriptors was used to express the solubility characteristics of these drugs. In order to verify the effectiveness of these compounds, we have to judge whether these compounds are the substrates of P-glycoprotein. According to the result, 2007_14247 and 2007_15317 are the substrates of P-glycoprotein. Considering the above factors, we selected 2007_13380, 2007_17103, and 2007_14247 as the possible compounds for the next experiment.

3.3 Artificial intelligence algorithms analysis

3.3.1 Adaptive boosting. The AdaBoost model was applied in this research and the strongly correlated features were selected for regression analysis. Regression prediction was

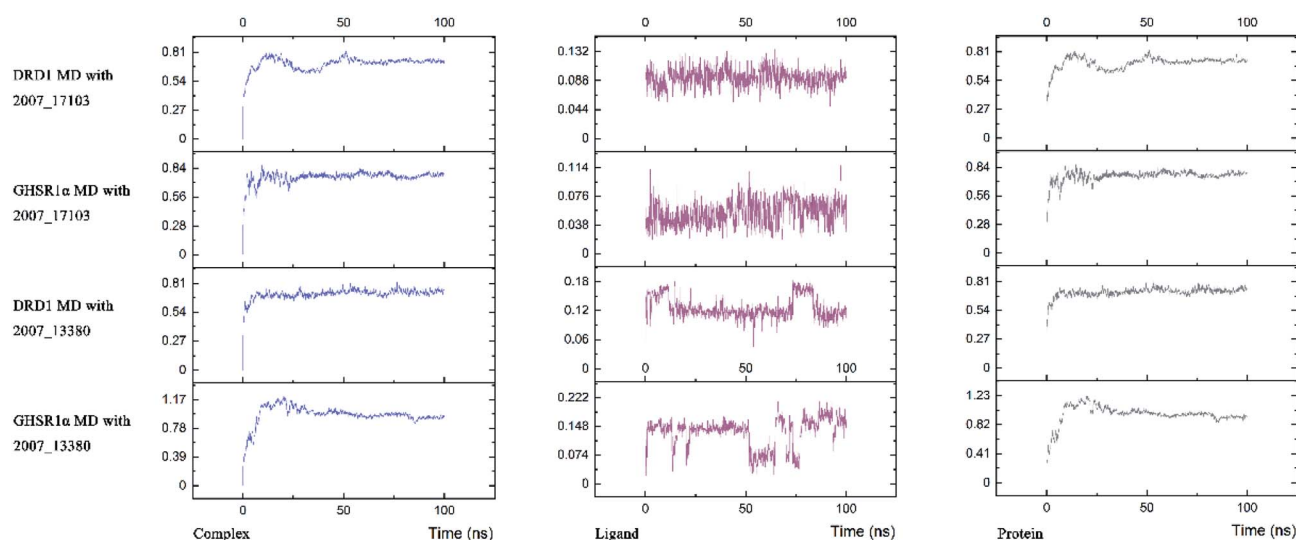


Fig. 15 RMSD curves of four molecular dynamics simulation experiments.



performed on the agonists datasets of the target protein GHSR1 α and AdaBoost achieved excellent experimental results. The *R*-square value of the training set and the test set reached 0.906 and 0.900, respectively. In the process of model building, we used 49 estimators as weak classifiers and used 20% of the data as the test set to check the rationality of model training. For the target protein DRD1, the *R*-square value of the training set and the test set reached 0.722 and 0.657, respectively. We tried a variety of combinations of weak classifiers and learning rates, and finally got the optimal value of the training result, including 16 estimators. The predictive activity results of these candidates are shown in Tables 4 and 5. According to the training results of this model, we believe that AdaBoost is more reliable for GHSR1 α agonists datasets. However, for DRD1 agonists datasets, AdaBoost does not perform well.

3.3.2 Gradient boosting. GB integrates many estimators, and finally, a strong classifier was obtained. The principle could be described as a new classifier fitting the residual of the previous classifier. In the process of GB training, we selected the decision tree as the weak classifier of the model, which has

strong adaptability to multi-feature data. There are as many as 204 molecular properties calculated by us. In order to reduce the redundant features and achieve reasonable prediction results, dimensionality reduction ought to be performed. According to our experimental results, the model achieves excellent prediction results when predicting DRD1 agonists. The *R*-square value of the training set and the test set reached 0.976 and 0.839, respectively. For GHSR1 α agonists, this model can also achieve relatively good results. The accuracy of the training set and the test set reached 0.935 and 0.785, respectively. Compared with AdaBoost, the prediction results of GB are more accurate. In addition, GB has better fitting capabilities for the agonists data sets of DRD1.

3.3.3 Support vector machine. We selected the RBF kernel function in our experiment, which can better handle small samples but not multi-character data sets. Our sample size is small but there are 204 molecular properties. Therefore, using the RBF kernel function-based SVM can better process the experimental data. The *R*-square value of the SVM model reached 0.942 and 0.708 for training set and test set in GHSR1 α

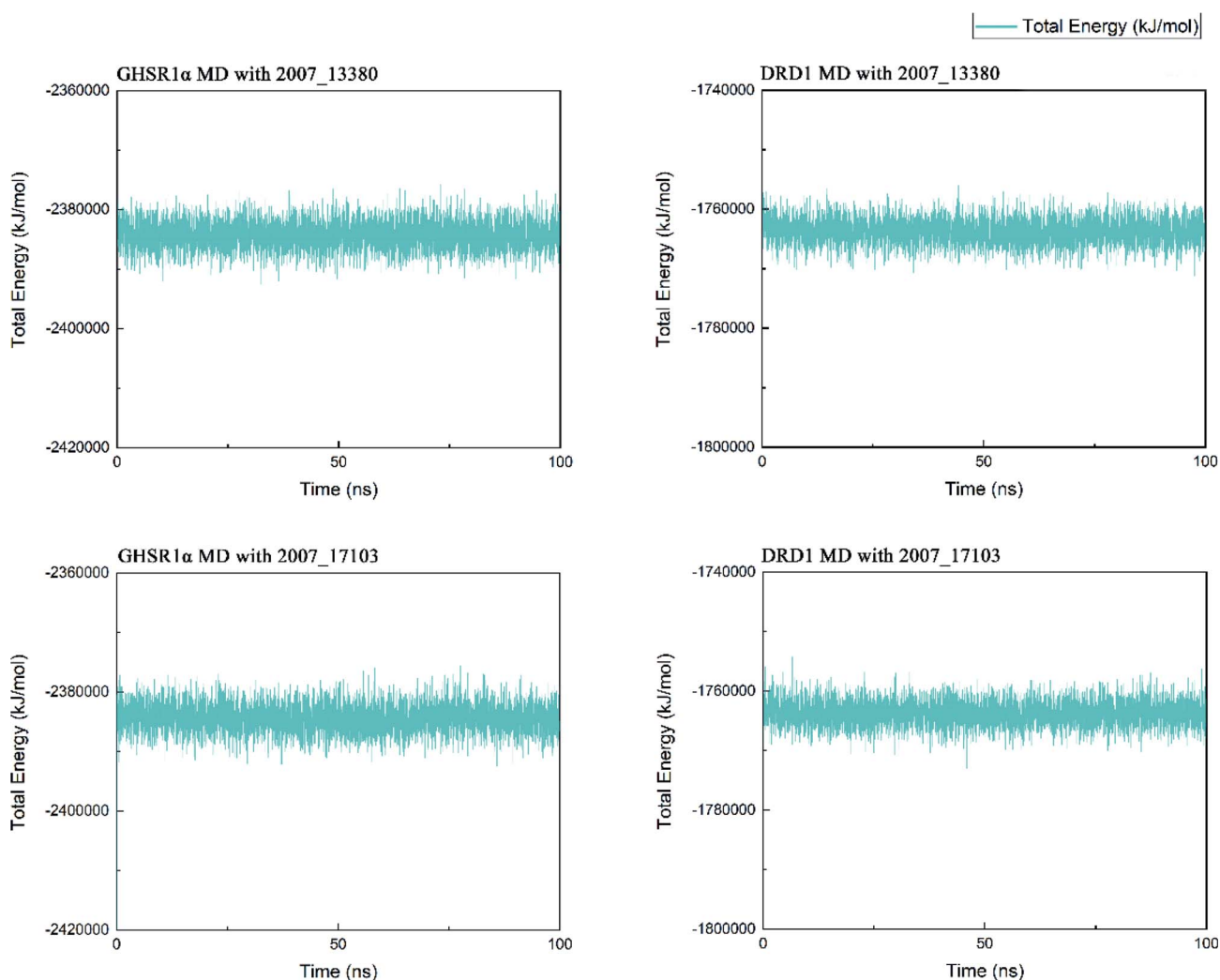


Fig. 16 The total energy curves of the complexes formed by the target proteins and ligands.



agonists data, respectively. According to the excellent prediction results for GHSR1 α agonists sets based on SVM, we believed that the prediction results of SVM are reliable. The *R*-squared of SVM reached 0.781 and 0.763 for the training set and the test set in DRD1 agonists data sets, respectively. Although the performance of SVM on the DRD1 agonists data sets is not satisfactory, we still believe that the prediction results are reliable, especially the fitting of SVM to complex feature data sets.

3.3.4 Random forest. RF model was also applied in this research. The RF model is composed of different classifiers too but each classifier uses the same algorithm and each classifier only selects a subset of the data set for training. In our experiment, the model was trained based on bagging. In the case of multiple sampling, bagging is more advantageous than pasting. Bagging will return samples after each sampling; however, pasting will discard the used samples. RF introduces more randomness into the decision trees and each classification is no

longer based on the best features. Thus, the decision tree has greater diversity, resulting in a better overall performance model. In the process of data preprocessing, the data features were selected in order to make the RF model more reliable. Finally, by adjusting the RF model, we got more accurate and reliable prediction results, which are shown in Tables 4 and 5.

3.3.5 Boost generalized regression neural network. Boost GRNN model was proposed by us in this article, which can be well applied to the training of small data sets and solves the problem of poor adjustability of the original GRNN model. There exist two modules in boost GRNN. The first module uses decision trees training the different subsets of dataset. It is worth mentioning that the data input to the decision trees was processed by bagging and each time a random subset is input for training, thereby ensuring the random diversity of the data. The second module consists of the part of the original GRNN model. We added a boost layer before the output layer to

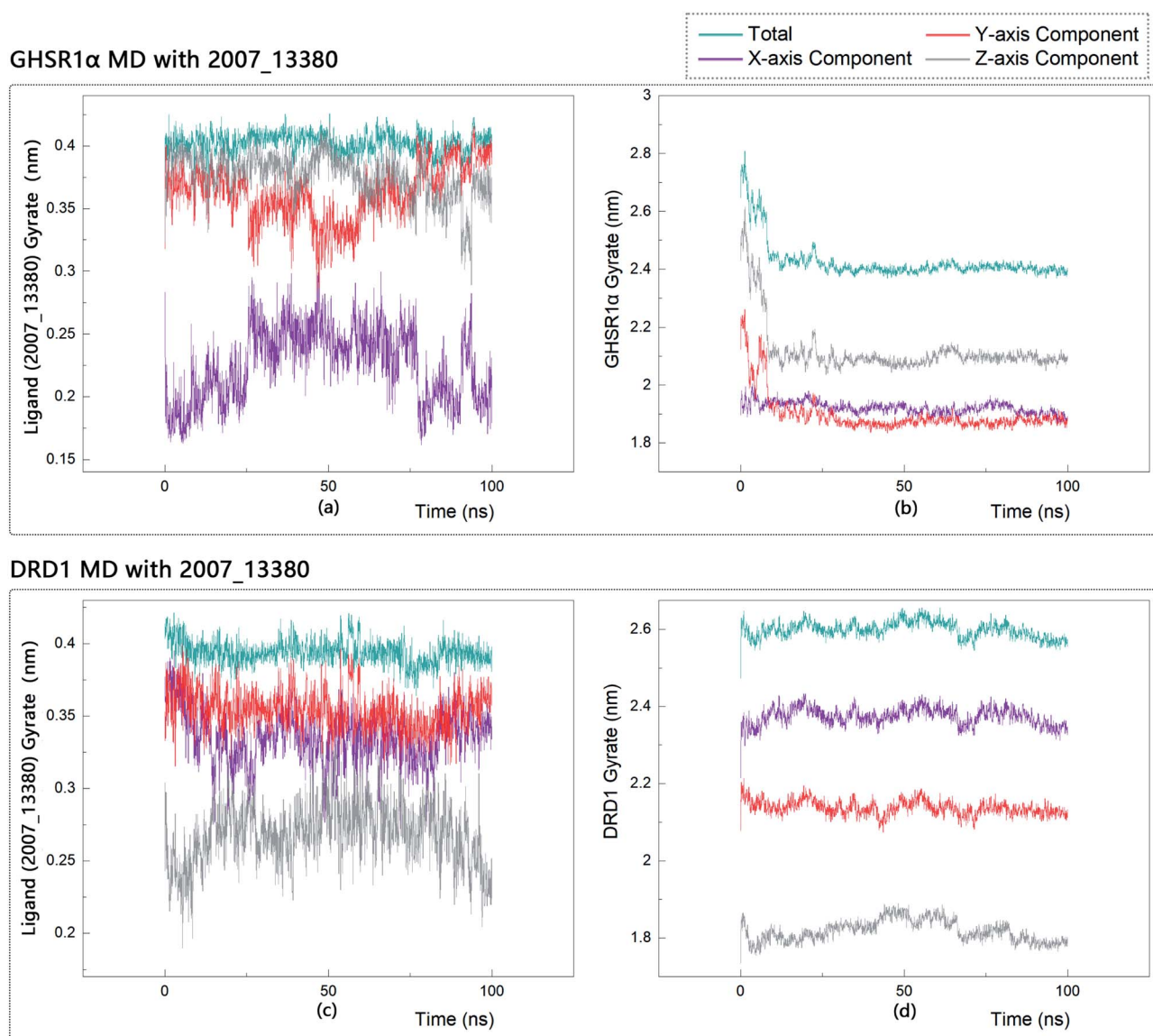


Fig. 17 Gyrate diagram of the complexes formed by GHSR1 α , DRD1, and 2007_13380.



comprehensively evaluate the predicted values obtained by the two modules. Good results were obtained for the two data sets based on boost GRNN. The results of boost GRNN shown that the R -square values of the test sets for the two data sets are higher than 0.8, which proves that boost GRNN has strong stability for small data set.

3.3.6 Elastic-net, linear ridge regression, stochastic gradient descent, and Lars Lasso. For small data sets, relatively good results were obtained from EN, LRR, SGD, and LL. The same feature selection criteria were applied to these models, and the feature selection was optimized for the characteristics of the four models. For the test set of GHSR1 α agonists, the mean square error (MSE) of the four models reached 0.09, 0.06, 0.12, and 0.06 respectively; for the test set of DRD1 agonists, the MSE of these models reached 0.06, 0.09, 0.09, and 0.2, respectively. In addition, the training results of LRR on GHSR1 α agonists reached 0.902 and 0.813 R -square for the training set and the test set, respectively.

The model evaluation results are shown in Table 6. The visualized training results are shown in Fig. 14. According to this diagram, we can obviously see that compared to other models, our boost GRNN model has better accuracy and the R -square values of the training sets reached 0.8 or more for data sets of both GHSR1 α and DRD1. Using artificial intelligence technology, we predict drug activity based on the features of the agonists of target proteins. In order to further explore the druggability of 2007_14247, 2007_17103, and 2007_13380, several MD experiments were performed to validate the stability of the protein-ligand complex.

3.4 Molecular dynamics simulation analysis

Three possible compounds that simultaneously interact with both GHSR1 α and DRD1 were selected for the 100 ns MD simulation experiments. MD results showed that only 2007_13380 and 2007_17103 could stably interact with the two

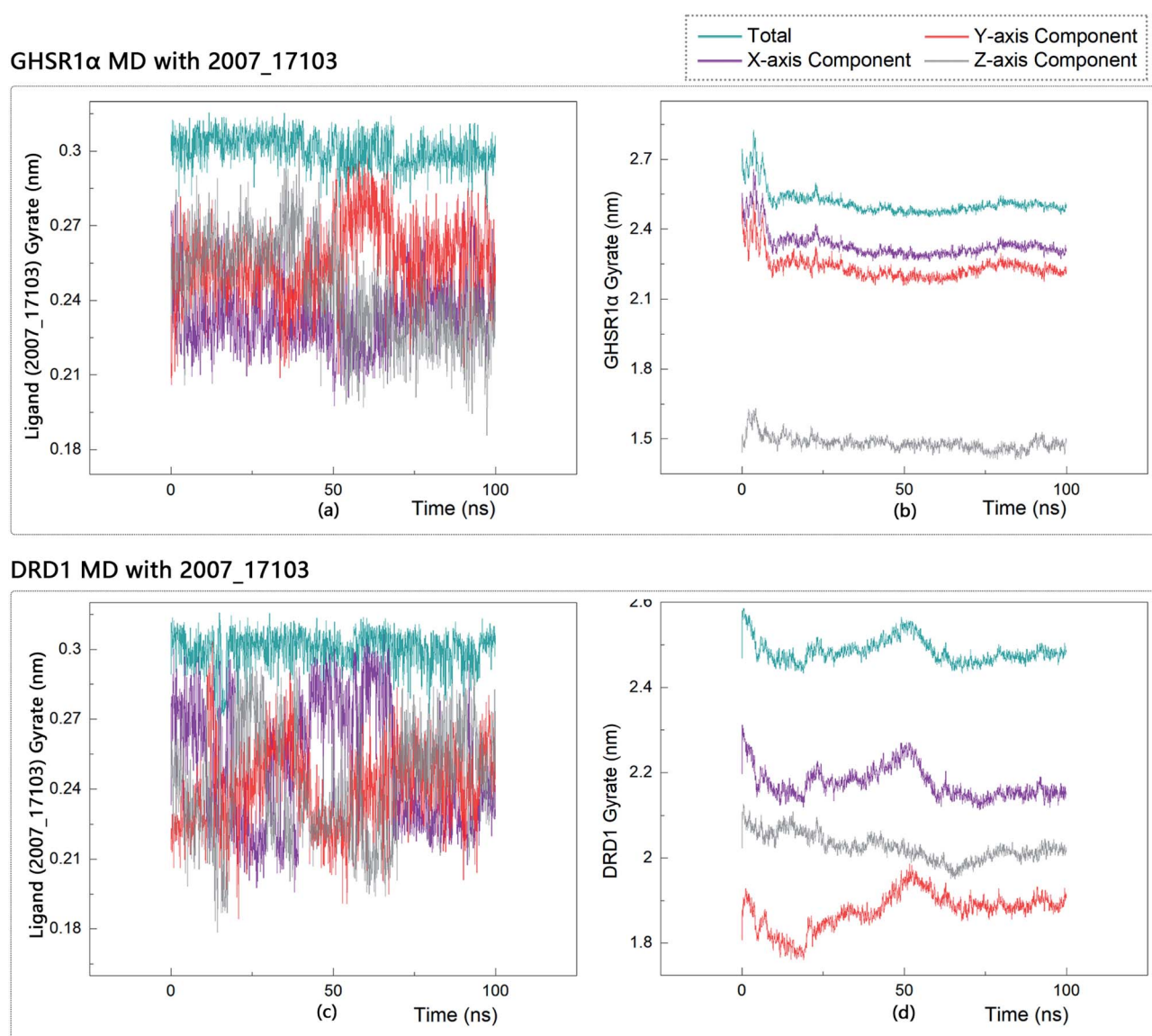


Fig. 18 Gyrate diagram of the complexes formed by GHSR1 α , DRD1, and 2007_17103.

target proteins, while 2007_14247 completely deviated from GHSR1 α during the process of MD. Therefore, the 2007_14247 cloud not interact with two target proteins stably. According to the results of RMSD analysis (Fig. 15), the RMSD curve of the complex formed by GHSR1 α and 2007_13380 had an obvious upward trend in the range of 0–20 ns and had obvious fluctuations in the range of 0–35 ns. We considered that the fluctuations of the RMSD curve of the complex might be cause by the change in the conformation because of the ligand bound into the target protein. At about the same time, the same situation appeared on the RMSD curves of the complexes formed by DRD1 and 2007_13380, GHSR1 α and 2007_17103, DRD1 and 2007_17103, respectively. Similarly, we considered that the same reason caused the same situation. Within 20–50 ns, there was a certain fluctuation in the RMSD curve of the complex composed of DRD1 and 2007_17103. It might be due to the change in the conformation of the complex after the ligand entered the target protein. However, fortunately, the RMSD curve returned to a calm and stable state after fluctuations. The RMSD curve of the complex formed by DRD1 and 2007_13380 almost showed a flat trend at 15–100 ns. These curves of the four

complexes eventually showed a state of convergence. In the MD simulation experiments of GHSR1 α , the RMSD of 2007_13380 fluctuated greatly, the RMSD curve of 2007_17103 was relatively stable and flat; in the MD simulation experiment of DRD1, the RMSD curve of 2007_13380 had a small fluctuation, and the curve of 2007_17103 was flat and stable. On the whole, compared to the RMSD curves of the complexes, the fluctuation of the RMSD curves of the ligands were negligible. The curves of the target proteins and the complexes had a great similarity; it can be shown that the target proteins have a larger effect of the overall RMSD curves trend. At the same time, we also analyzed the total energy of the four simulation experiments. The results showed that the total energy of the system in these MD simulation experiments were stable, which were maintained between $-2\,390\,000$ KJ mol $^{-1}$ to $-2\,380\,000$ KJ mol $^{-1}$, $-1\,777\,000$ KJ mol $^{-1}$ to $-1\,760\,000$ KJ mol $^{-1}$, $-2\,390\,000$ KJ mol $^{-1}$ to $-2\,380\,000$ KJ mol $^{-1}$ and $-1\,777\,000$ KJ mol $^{-1}$ to $-1\,760\,000$ KJ mol $^{-1}$, respectively. The diagrams of total energy are shown in Fig. 16.

The radius of gyration reflects the volume and shape of the complex. The larger the radius of gyration, the more expansion

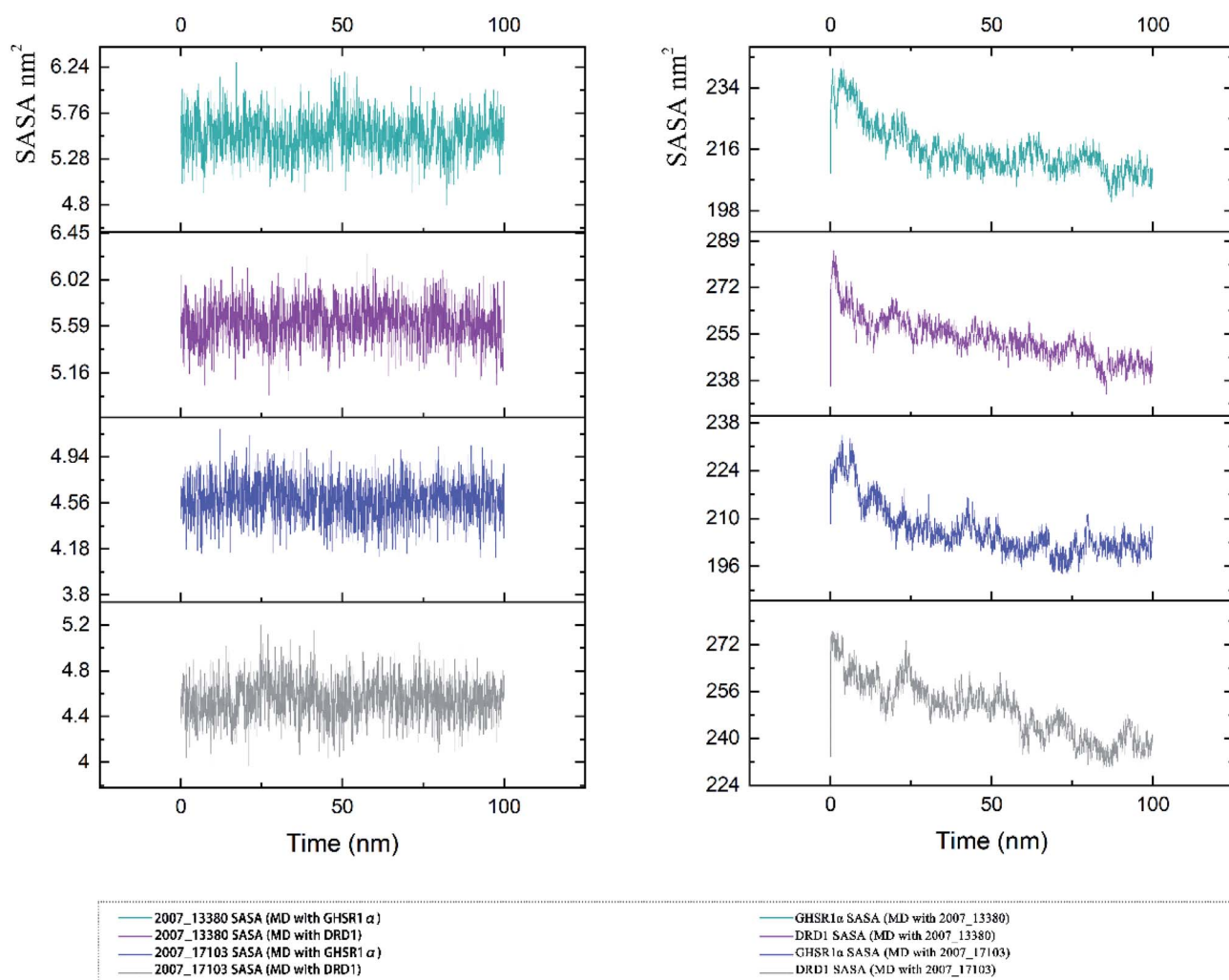


Fig. 19 SASA analysis of the target proteins and ligands.



of the complex. We calculated the gyration radius of the total, X axis, Y axis, and Z axis. From our experimental results of gyration, it could be seen that during 0–15 ns, the rotation rate of GHSR1 α showed a rapid decline (Fig. 17b and 18b), which indicated that the GHSR1 α protein structure was tightening rapidly during the process of MD simulation; the gyration curve of DRD1 was relatively flat in the experiment of DRD1 MD with 2007_13380 (Fig. 17d) while the DRD1 gyration curve has a great fluctuation in the experiment of DRD1 MD with 2007_17103 (Fig. 18d) during 0–65 ns. Fortunately, the curves tend to be stable in the range of 65–100 ns. In the range of 15–100 ns, the gyration curve of GHSR1 α MD with 2007_13380 (Fig. 17b) tended to be flat; the gyration curve of GHSR1 α MD with 2007_17103 (Fig. 18b) has a slight fluctuation close to flat. Ligands MD with GHSR1 α , X axis, Y axis, and Z axis curves fluctuated greatly for both GHSR1 α MD with 2007_13380 and GHSR1 α MD with 2007_17103; fortunately, the decisive indicator total curves are nearly flat (Fig. 17a and 18a). In the experiment of DRD1 MD with 2007_13380, the gyration curves of 2007_13380 (Fig. 17c), total, X axis, and Y axis curves are relatively stable; however, the curve of Z axis has a certain range

of fluctuations. In the experiment of DRD1 MD with 2007_17103, there existed fluctuations in the X axis, Y axis, and the Z axis (Fig. 18c), while the total curve tended to be flat. Generally speaking, although there are fluctuations of different amplitudes on the X axis, Y axis, and Z axis, the decisive indicator total components tend to be stable; thus, we have reason to believe that ligand binding in the protein is relatively stable.

The SASA indicator helped us to judge the hydrophobicity of the protein and the state of the protein surface. We calculated the SASA data of the four MD experiments of GHSR1 α and DRD1 (Fig. 19). The SASA results showed that the ligands were quite stable in these MD experiments and the SASA curves of the two target proteins dropped sharply at 0–50 ns. However, the SASA curves tend to be flat at 50–100 ns. The results of SASA further demonstrated that during the simulation timescale, the ligand–protein complexes formed by the target proteins and candidates are stable.

The RMSF indicator was used to evaluate the variation of each residue in these simulation experiments. The higher the RMSF value, the more unstable the residue is. In other words, the residue changed greatly before and after the simulation

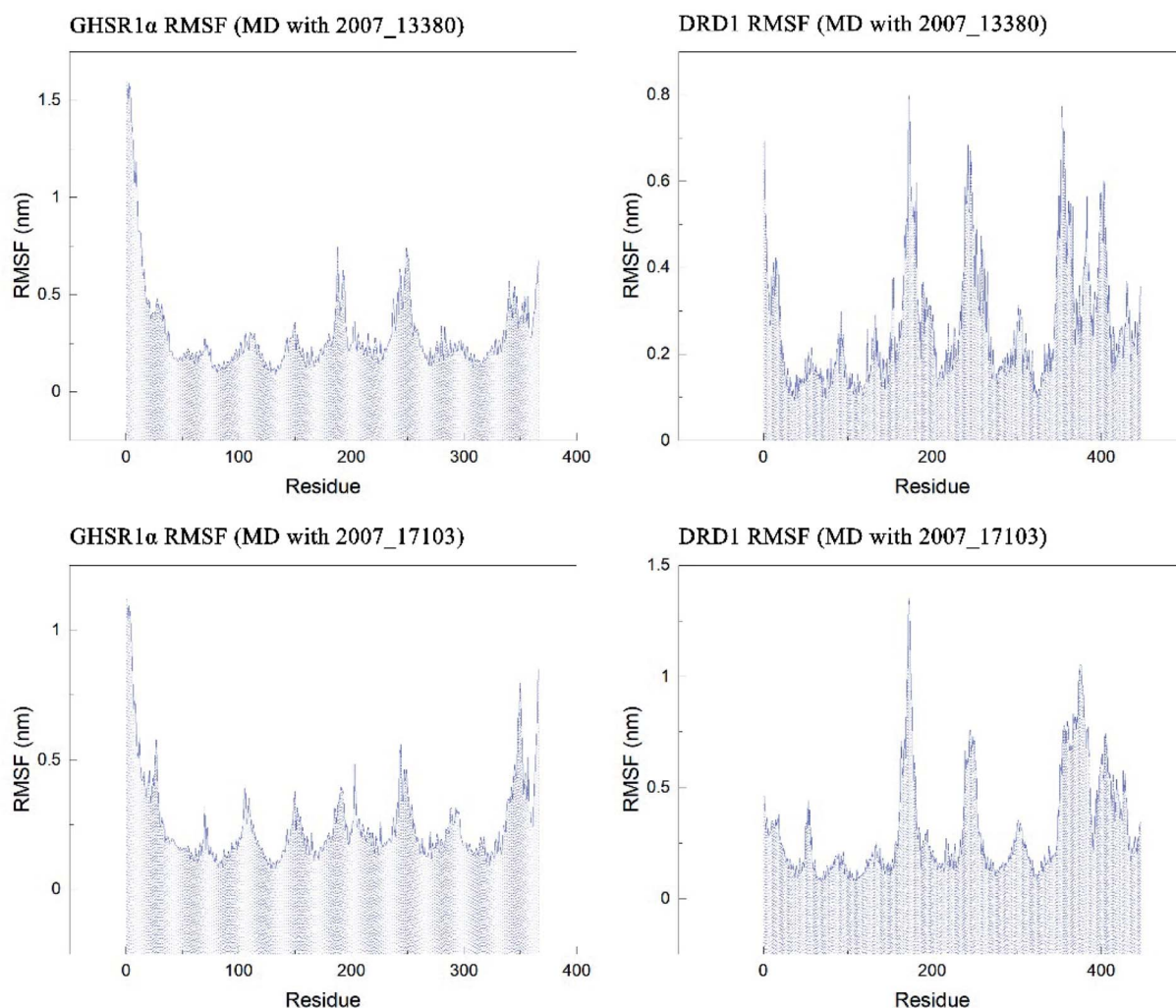


Fig. 20 RMSF curves of the target proteins and ligands.



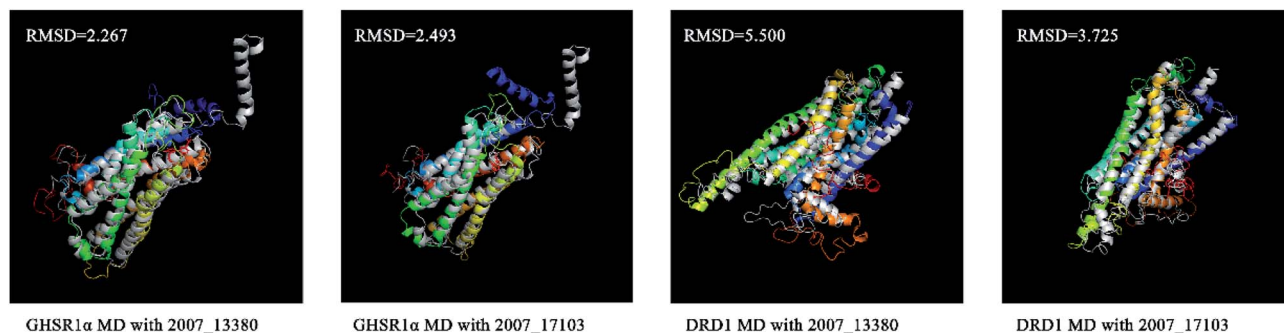


Fig. 21 Superposition diagrams of the initial (silver) and final structures of the target proteins.

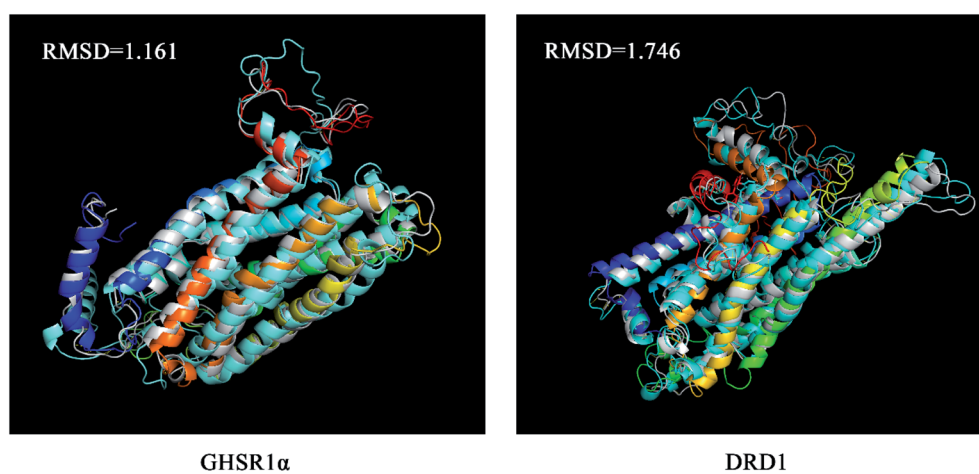


Fig. 22 The average structure (silver) and the final state structure were superimposed to obtain the RMSD values.

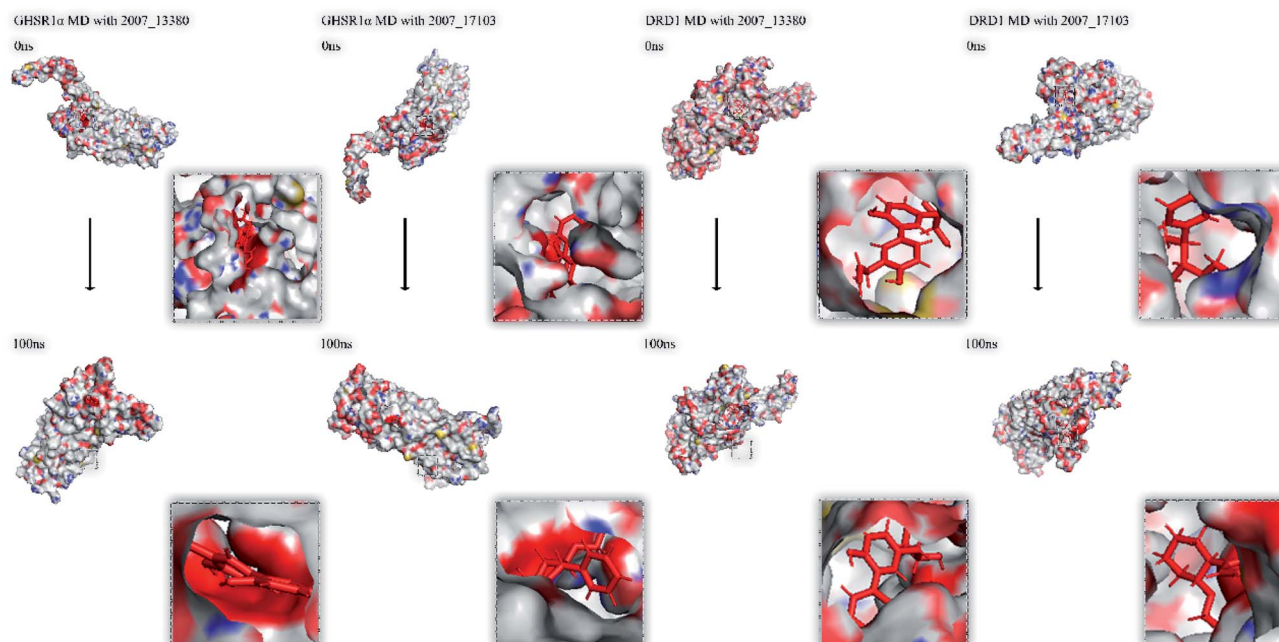


Fig. 23 Comparison diagram before and after molecular dynamics simulation.



experiments. We calculated the RMSF values of the two target protein residues, as shown in Fig. 20. From the RMSF curve diagram, we could see that the GHSR1 α residues behave well overall in the experiment of MD with 2007_13380 and there exist local residues with poor stability; residues in the range of 0–25 and 340–366 had higher RMSF values when MD with 2007_17103 was performed. For the MD simulation experiment of DRD1 and 2007_13380, there exist two ranges of 150–250 ns and 350–400 ns in which the stability of the residues was poor; the last picture of the RMSF curves showed that a small number of residues in the tail of DRD1 was unstable.

We superimposed these proteins obtained from the simulation experiments and used the RMSD indicator to evaluate these conformations. The conformations of GHSR1 α and DRD1 before and after the experiment were superimposed, which are shown in Fig. 21. The RMSD of GHSR1 α superposition structures reached 2.267 and 2.493 for the MD experiments of 2007_13380 and 2007_17103, respectively. The RMSD of DRD1 superposition structures reached 5.500 and 3.725 for the MD experiments of 2007_13380 and 2007_17103, respectively.

The superimposed results of the average structure and the final conformation obtained from the MD experiments are shown in Fig. 22. Both GHSR1 α and DRD1 achieved good superposition results reaching 1.161 and 1.746, respectively, which indicate that these structures have great similarities.

Finally, we drew the comparison diagram of the conformational changes of the complexes in the four MD experiments (Fig. 23). From the diagram, we can clearly see that all the ligands are still firmly bound to the target proteins in the protein at the end of the MD simulation experiments.

4 Conclusion

Overall, relying on the world's largest TCM database and the versatile artificial intelligence technology, we have found the Chinese medicine ingredients suitable for AD. The prediction results of artificial intelligent models show that 2007_14247, 2007_17103, 2007_13380, 2007_7588, and 2007_15317 have high drug activity. In order to verify whether the prediction results are reliable, we performed MD simulation experiments simulating 2007_14247, 2007_13380, and 2007_17103 with GHSR1 α and DRD1. 2007_14247 was detached from GHSR1 α . 2007_13380 and 2007_17103 still binds to the two target proteins stably. Therefore, we consider that 2007_13380 and 2007_17103 are the possible multi-target candidates for AD.

Author contributions

Calvin Yu-Chian Chen designed research. Zi-Qiang Tang, Lu Zhao worked together to complete the experiment and analyzed the data. Calvin Yu-Chian Chen, Lu Zhao contributed to analytic tools. Zi-Qiang Tang, Lu Zhao, and Calvin Yu-Chian Chen wrote the manuscript together.

Conflicts of interest

The author reports no conflicts of interest in this work.

Acknowledgements

This work was supported by Guangzhou Science and Technology fund (Grant No. 201803010072), Science, Technology and Innovation Commission of Shenzhen Municipality (JCYL 20170818165305521) and China Medical University Hospital (DMR-110-097). We also acknowledge the start-up funding from SYSU "Hundred Talent Program".

References

- 1 H. Parmar, B. Nutter, R. Long, S. Antani and S. Mitra, *J. Med. Imaging*, 2020, **7**, 1–14.
- 2 S. Simpraga, R. Alvarez-Jimenez, H. D. Mansvelder, J. M. A. van Gerven, G. J. Groeneveld, S.-S. Poil and K. Linkenkaer-Hansen, *Sci. Rep.*, 2017, **7**, 5775.
- 3 S. W. Scheff, D. A. Price, F. A. Schmitt and E. J. Mufson, *Neurobiol. Aging*, 2006, **27**, 1372–1384.
- 4 J. Tian, L. Guo, S. Sui, C. Driskill, A. Phensy, Q. Wang, E. Gauba, J. M. Zigman, R. H. Swerdlow, S. Kroener and H. Du, *Sci. Transl. Med.*, 2019, **11**, eaav6278.
- 5 G. Navarro, D. Aguinaga, E. Angelats, M. Medrano, E. Moreno, J. Mallol, A. Cortés, E. I. Canela, V. Casadó and P. J. McCormick, *J. Biol. Chem.*, 2016, **291**, 13048–13062.
- 6 A. Kern, M. Mavrikaki, C. Ullrich, R. Albarran-Zeckler, A. F. Brantley and R. G. Smith, *Cell*, 2015, **163**, 1176–1190.
- 7 A. Kern, C. Grande and R. G. Smith, *Front. Endocrinol.*, 2014, **5**, 129.
- 8 T. Abel, P. V. Nguyen, M. Barad, T. A. Deuel, E. R. Kandel and R. J. C. Bourtoouladze, *Cell*, 1997, **88**, 615–626.
- 9 Y.-C. Chen, *Trends Pharmacol. Sci.*, 2015, **36**, 78–95.
- 10 T.-Y. Tsai, K.-W. Chang and C. Y.-C. Chen, *J. Comput.-Aided Mol. Des.*, 2011, **25**, 525–531.
- 11 K.-W. Chang, T.-Y. Tsai, K.-C. Chen, S.-C. Yang, H.-J. Huang, T.-T. Chang, M.-F. Sun, H.-Y. Chen, F.-J. Tsai and C. Y.-C. Chen, *J. Biomol. Struct. Dyn.*, 2011, **29**, 243–250.
- 12 C. Y.-C. Chen, *PLoS One*, 2011, **6**, e15939.
- 13 M. Hassan Baig, K. Ahmad, S. Roy, J. Mohammad Ashraf, M. Adil, M. Haris Siddiqui, S. Khan, M. Amjad Kamal, I. Provaznik and I. Choi, *Curr. Pharm. Des.*, 2016, **22**, 572–581.
- 14 S. Ekins, A. C. Puhl, K. M. Zorn, T. R. Lane, D. P. Russo, J. J. Klein, A. J. Hickey and A. M. Clark, *Nat. Mater.*, 2019, **18**, 435–441.
- 15 X. Wang, B. Yu, A. Ma, C. Chen, B. Liu and Q. Ma, *Bioinformatics*, 2019, **35**, 2395–2402.
- 16 E. Lounkine, M. J. Keiser, S. Whitebread, D. Mikhailov, J. Hamon, J. L. Jenkins, P. Lavan, E. Weber, A. K. Doak and S. Côté, *Nature*, 2012, **486**, 361–367.
- 17 X. Yang, Y. Wang, R. Byrne, G. Schneider and S. Yang, *Chem. Rev.*, 2019, **119**, 10520–10594.
- 18 A. Khan, S. S. Ali, M. T. Khan, S. Saleem, A. Ali, M. Suleman, Z. Babar, A. Shafiq, M. Khan and D.-Q. Wei, *J. Biomol. Struct. Dyn.*, 2020, 1–12.
- 19 S. A. Hollingsworth and R. O. Dror, *Neuron*, 2018, **99**, 1129–1143.



- 20 G. Bitencourt-Ferreira, A. D. da Silva and W. F. de Azevedo, *Curr. Med. Chem.*, 2020, 253–265.
- 21 E. Altermann and T. R. Klaenhammer, *BMC Genomics*, 2005, 6, 60.
- 22 P. Shannon, A. Markiel, O. Ozier, N. S. Baliga, J. T. Wang, D. Ramage, N. Amin, B. Schwikowski and T. Ideker, *Genome Res.*, 2003, 13, 2498–2504.
- 23 R. K. Sunahara, H. B. Niznik, D. M. Weiner, T. M. Stormann, M. R. Brann, J. L. Kennedy, J. Gelernter, R. Rozmahel, Y. Yang and Y. Israel, *Nature*, 1990, 347, 80–83.
- 24 R. G. Smith, R. J. Leonard, A. R. T. Bailey, O. C. Palyha, S. D. Feighner, C. Tan, K. K. Mckee, S. Pong, P. R. Griffin and A. D. Howard, *Endocrine*, 2001, 14, 9–14.
- 25 R. Apweiler, A. M. Bairoch, C. H. Wu, W. C. Barker, B. Boeckmann, S. Ferro, E. Gasteiger, H. Huang, R. Lopez and M. Magrane, *Nucleic Acids Res.*, 2004, 32, 115–119.
- 26 J. Yang and Y. Zhang, *Curr. Protoc. Bioinf.*, 2015, 52, 5.8.1–5.8.15.
- 27 J. Yang, R. Yan, A. Roy, D. Xu, J. Poisson and Y. Zhang, *Nat. Methods*, 2015, 12, 7–8.
- 28 W. Zheng, C. Zhang, E. W. Bell and Y. Zhang, *Future Gener. Comput. Syst.*, 2019, 99, 73–85.
- 29 J. Yang and Y. Zhang, *Nucleic Acids Res.*, 2015, 43, W174–W181.
- 30 S. Thangapandian, S. John, S. Sakkiah and K. W. Lee, *J. Chem. Inf. Model.*, 2011, 51, 33–44.
- 31 R. H. Khan, M. K. Siddiqi, V. N. Uversky and P. Salahuddin, *Int. J. Biol. Macromol.*, 2019, 127, 250–270.
- 32 C. M. Venkatachalam, X. Jiang, T. Oldfield and M. Waldman, *J. Mol. Graphics Modell.*, 2003, 21, 289–307.
- 33 K. Vanommeslaeghe, E. Hatcher, C. Acharya, S. Kundu, S. Zhong, J. Shim, E. Darian, O. Guvench, P. E. M. Lopes and I. Vorobyov, *J. Comput. Chem.*, 2009, 31, 671–690.
- 34 B. R. Brooks, C. L. Brooks, A. D. Mackerell, L. Nilsson, R. J. Petrella, B. Roux, Y. Won, G. Archontis, C. Bartels and S. Boresch, *J. Comput. Chem.*, 2009, 30, 1545–1614.
- 35 B. R. Brooks, R. E. Bruccoleri, B. D. Olafson, D. J. States, S. Swaminathan and M. Karplus, *J. Comput. Chem.*, 1983, 4, 187–217.
- 36 A. Ghaleb, A. Aouidate, H. B. E. Ayouchia, M. Aarjane, H. Anane and S.-E. Stiriba, *J. Biomol. Struct. Dyn.*, 2020, 1–11.
- 37 H. van de Waterbeemd and E. Gifford, *Nat. Rev. Drug Discovery*, 2003, 2, 192–204.
- 38 A. Daina, O. Michielin and V. Zoete, *Sci. Rep.*, 2017, 7, 42717.
- 39 A. Gaulton, L. J. Bellis, A. P. Bento, J. Chambers, M. Davies, A. Hersey, Y. Light, S. McGlinchey, D. Michalovich and B. Al-Lazikani, *Nucleic Acids Res.*, 2012, 40, D1100–D1107.
- 40 G. Papadatos, A. Gaulton, A. Hersey and J. P. Overington, *J. Comput.-Aided Mol. Des.*, 2015, 29, 885–896.
- 41 P. Sedgwick, *BMJ*, 2012, 345, e4483.
- 42 T. Hastie, S. Rosset, J. Zhu and H. Zou, *Stat. Its Interface*, 2009, 2, 349–360.
- 43 L. Deng, W. Yang and H. Liu, *Front. Genet.*, 2019, 10, 637.
- 44 J. Friedman, T. Hastie and R. Tibshirani, *J. Stat. Softw.*, 2010, 33, 1.
- 45 A. Schneider, G. Hommel and M. Blettner, *Dtsch. Arztebl. Int.*, 2010, 107, 776.
- 46 H. Asai, S. Tanaka and K. Uegima, *IEEE Trans Syst Man Cybern Syst*, 1982, 12, 903–907.
- 47 M. A. Hearst, S. T. Dumais, E. Osuna, J. Platt and B. Scholkopf, *IEEE Intell. Syst.*, 1998, 13, 18–28.
- 48 A. J. Smola and B. Scholkopf, *Stat. Comput.*, 2004, 14, 199–222.
- 49 M. W. Huang, C. W. Chen, W. C. Lin, S. W. Ke and C. F. Tsai, *PLoS One*, 2017, 12, e0161501.
- 50 B. Kuo, H. Ho, C. Li, C. Hung and J. S. Taur, *IEEE J. Sel. Top. Appl. Earth Obs. Remote Sens.*, 2014, 7, 317–326.
- 51 L. Wang, Y. Yang, R. Min and S. Chakradhar, *Neural Netw.*, 2017, 93, 219–229.
- 52 C. Khanji, L. Lalonde, C. Bareil, M.-T. Lussier, S. Perreault and M. Schnitzer, *Med. Care*, 2019, 57, 63–72.
- 53 A. Avdeef, *ADMET DMPK*, 2020, 8, 29–77.
- 54 Y. Chtioui, S. Panigrahi and L. Francl, *Chemom. Intell. Lab. Syst.*, 1999, 48, 47–58.
- 55 R. G. Smith, L. H. Van der Ploeg, A. D. Howard, S. D. Feighner, K. Cheng, G. J. Hickey, M. J. Wyratt Jr, M. H. Fisher, R. P. Nargund and A. A. Patchett, *Endocr. Rev.*, 1997, 18, 621–645.
- 56 M. M. Lewis, V. J. Watts, C. P. Lawler, D. E. Nichols and R. B. Mailman, *J. Pharmacol. Exp. Ther.*, 1998, 286, 345–353.
- 57 B. Bayel Secinti, G. Tatar and T. Taskin Tok, *J. Biomol. Struct. Dyn.*, 2019, 37, 2457–2463.

